COMMUNICATION

ADVANCED
MATERIALS
TECHNOLOGIES

www.advmattechnol.d

Check for
updates

Distortion-Free Stretchable Light-Emitting Diodes via Imperceptible Microwrinkles

Sujin Jeong, Hyungsoo Yoon, Byeongmoon Lee, Seunghwan Lee, and Yongtaek Hong*

Stretchable organic light-emitting diodes (OLEDs) have been considered as a promising technology for next-generation free-form and wearable displays. However, an approach to ensure both high device performance and high resolution has not yet been suggested. While introducing a wrinkled structure in the active pixel areas is a decent method, the formation of out-of-plane macroscopic wrinkles having a wavelength of a few hundred μm has caused distortion in the shape of the pixel, which is a critical drawback for a matrix-configured display demanding a sharp pixel definition. Herein, microwrinkled OLEDs are fabricated to define a distortion-free pixel by direct deposition of OLEDs on biaxially prestretched elastomeric substrate, being feasible by a low-temperature-based solution process. The total thickness of the device can be significantly reduced up to 350 nm, producing the imperceptible microwrinkles having a wavelength under 20 μm. The microwrinkled OLEDs show a luminance over 8000 cd m^{-2} and maximum current efficiency of 7.76 cd A^{-1}, which is comparable to the device without wrinkled structure. Finally, a stretchable 4 × 4 OLED pixel array with a microwrinkled structure is demonstrated showing sharply defined square-patterned emission, proving the potential in the future high-resolution stretchable display.

Stretchable light-emitting devices (LEDs) are expected to pave the way for a novel form-factor of the next-generation display, beyond the flat panel displays. Stretchable LEDs can extend the applicable areas of display by shaping onto arbitrary surfaces[1,2] or by enabling a novel type of wearable displays, such as a textile display[3] or a contact lens display.[4] Enabling technologies of stretchable LEDs can be categorized into two types: material-based approach and geometric approach. The material-based approach is utilizing intrinsically stretchable materials as active layers in LED structure, while still in the research phase that explores the possibilities of various materials. Due to their simple device structures and development of appropriate soft materials, light-emitting electrochemical cells (LEC)[5,6] and alternating current electroluminescence (ACEL)[7] have been suggested as great candidates for intrinsically stretchable LEDs. However, the device performances are much lower than the

conventional LEDs, which is far behind the implementation of wearable devices.

On the other hand, geometric approaches exploit structural engineering that absorbs the applied strain to prevent LEDs from being directly stretched. By applying appropriate structural designs to the conventional high-modulus materials and LED arrays, the conventional LEDs can have stretchability without replacing the materials. One of the representative structural designs is connecting the LEDs placed at the stress-free island areas to stretchable interconnects, so-called island-bridge structure. Metallic-based electrodes using serpentine structure,[8] metallic nanoparticles embedded in a soft matrix,[9] or vertically wavy structure[10] were reported as candidates for stretchable interconnects. However, because the stretchable interconnect that occupies the area between the adjacent islands determines the stretchability of the system, insufficient space for the interconnects results in reduced stretchability due to the highly concentrated strain. This is the major bottleneck in increasing spatial resolution of stretchable displays.

Another structural design is to form a wavy buckling/wrinkle structure in the active pixels of thin-film-based LEDs (TFLED).[11–20] Using this method, the pixel itself appears to be stretched, similar to intrinsically stretchable LEDs, so that the display resolution can be increased without the loss of area occupied by interconnects. For wrinkled structure, TFLEDs are fabricated on an ultrathin plastic film (e.g., polyethylene terephthalate (PET), polyethylene naphthalate (PEN), polyimide (PI)) with a thickness of under tens of micrometers, and the entire device including the plastic film is transferred to the prestretched elastomer by laminating the peeled-off freestanding device. Then, by releasing a prestrain, the wrinkle structure can be formed. This indirect method allows the fabrication of stretchable LEDs without changing the conventional OLED depositing techniques. Previous research about wrinkled TFLEDs reported that the electrooptical properties are maintained before and after the formation of wrinkle structure. However, during the transfer process, handling of ultrathin thin-film-based LEDs, of which the thickness is about several μm to tens of μm, is quite intricate. Air bubbles can be trapped or the unexpected pressure can be applied to the TFLEDs, which causes low-yield issues during a lamination process.[21] Moreover, the most problematic issue is the formation of large-sized

S. Jeong, H. Yoon, B. Lee, S. Lee, Prof. Y. Hong
Department of Electrical and Computer Engineering
Inter University Semiconductor Research Center (ISRC)
Seoul National University
Seoul 08826, Republic of Korea
E-mail: yongtaek@snu.ac.kr

The ORCID identification number(s) for the author(s) of this article can be found under https://doi.org/10.1002/admt.202000231.

**ADVANCED
SCIENCE NEWS**
www.advancedsciencenews.com

**ADVANCED
MATERIALS
TECHNOLOGIES**
www.advmattechnol.de

deep wrinkles having a wavelength of a few hundred µm, which are perceptible to the naked eyes. To the best of our knowledge, all the previous research about stretchable TFLEDs with wrinkled structure reported a formation of a macroscopic wrinkle, which is a major obstacle to practical use in display applications causing a distortion in images. The pixels on the out-of-plane wavy structure are observed to be bumpy and the deep wrinkles along the edge of the pixel irregularly deform the shape of the pixel, which is not suitable for a matrix-configured display that demands a sharp pixel definition. In particular, while 2D wrinkles are preferred for mechanical durability in the multiaxial directions, 2D oriented random wrinkles formed by a biaxial prestretching cause more acute distortion by the formation of disordered wrinkles,[12,15,22] compared to periodic straight wrinkles formed by a uniaxial prestretching.

Herein, imperceptibly microwrinkled organic light-emitting diodes (OLEDs) to define distortion-free pixel is reported by direct deposition of OLEDs on biaxially prestretched elastomeric polydimethylsiloxane (PDMS) substrate without the aid of ultrathin plastic film. Through this approach, not only the possible issues occurred during the transfer process can be prevented, but also the total thickness of the high-modulus film can be decreased enabling a formation of microwrinkled structure. Hereafter, "wavelength" and "amplitude" of wrinkles will be used to identify the feature of the micro and macrowrinkles,[15–17,19] where the same structural character of the wrinkles is also identified as "peak-to-peak distance"[11] or "period"[13,18,20] as well. To date, the wavelength of wrinkles has not been considered as a controllable factor and discussed only when analyzing bending strain induced to the device.[11,12,15,16,19] The wavelength of wrinkles can be modulated to imperceptible level through our approach. Furthermore, the microwrinkles can relieve the out-of-plane wavy structure, solving the distortion effect caused by a formation of complex and macroscopic wrinkles (**Figure 1**a).

The formation of wrinkles is determined by a nonlinear buckling theory.[23] Wavelength and amplitude of wrinkles are determined by a result of the minimization of deformation energy applied to a stiff film placed on a soft elastomeric substrate. In 1D wrinkling case, the wavelength of the wrinkle follows Equation (1)[23]

$$\lambda \propto 2\pi h_{f} \left(\frac{\overline{E_{f}}}{3\overline{E_{s}}} \right)^{\frac{1}{3}} \qquad (1)$$
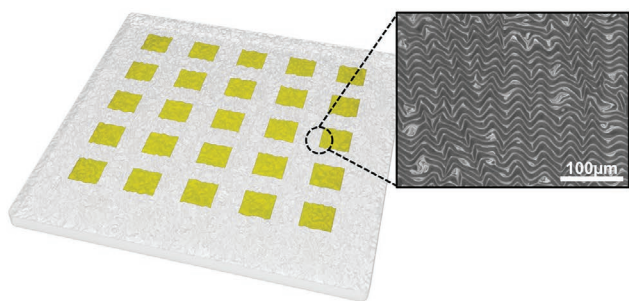
Here, λ is the wavelength, h is the thickness, and $\overline{E}$ is the plane-strain modulus, where the subscripts of f and s represent a film and substrate, respectively. According to the above relationship, the wavelength is proportional to the thickness of the film. Therefore, by reducing the thickness of the film deposited on the prestretched elastomer, fine wrinkles can be obtained. More complex morphologies generated in 2D wrinkling case cannot be simply explained by the above mechanic model.[24] However, except that complex patterns are formed by deformation in multiple directions, it is clear that the film thickness has a similar effect on the wavelength of wrinkles in the bidirectional prestretching. Therefore, it can be inferred that reducing the film thickness is a key factor in overcoming the distortion effect that arises from the topography of the wrinkled structure.

In the conventional process of fabricating wrinkled LEDs, transfer printing the OLEDs fabricated on a thin plastic film to the prestretched elastomer is a well-known method as mentioned above. However, the thickness of the plastic film, which is laminated to the elastomer, is a limiting factor in reducing the total thickness of the device making it difficult to shorten the wavelength of wrinkle structure to the imperceptible level. In previous studies, the total thickness of the device has been over 1.5 µm, resulting in the wavelength of a wrinkled structure at least 100 µm, which is perceptible to naked eyes. Some studies using the periodic template for highly engineered wrinkles showed high mechanical stability, but the wavelength of the wrinkles even exceeded 400 µm, which can distort the displaying images (Figure 1b and Table S1 in the Supporting Information).[13,18,20] In this work, the film thickness on elastomer was significantly reduced by removing the laminated plastic film and by directly depositing solution-processed polymer LEDs (PLEDs) on the prestretched PDMS. The fabricated device structure is described in Figure 1c, where the active layers of poly(3,4-ethylenedioxythiophene):poly(styrenesulfonate) (PEDOT:PSS, anode)/PEDOT:PSS (HIL)/Super yellow (EML)/polyethylenimine (PEI, interlayer)/zinc oxide nanoparticles (ZnO, EIL)/aluminum (Al, cathode) are directly deposited on PDMS substrate. The total thickness of PLEDs on PDMS is 340 nm, which is one-third of the previous studies, considering that the thinnest plastic film reported in the previous research was about 1–1.5 µm,[11,14–17] opening up the feasibility of a microwrinkled PLEDs.

So far, fabricating OLEDs directly on a PDMS substrate has been suffered from thermal expansion and low surface energy issues. PDMS has a thermal expansion coefficient of 3.1×10^{-4} °C^{-1}, making the deposited thin films vulnerable to heat-induced thermal expansion during the fabrication process, leading to the formation of wrinkles or cracks.[25–27] It is necessary to employ low-temperature-based solution process. In the fabrication process, the maximum process temperature is set at 120 °C, which is an endurable level where no deformations occur. Besides, to deposit a thin film on a PDMS substrate, its intrinsic hydrophobic nature and fast hydrophobic recovery after surface treatment should be considered and process condition should be delicately optimized.[28] The detailed fabrication process is described in Figure 1d and the Experimental Section. At first, a biaxially prestretched PDMS fixed to a carrier glass substrate is prepared. The biaxial prestrain of 20% was applied in this work if a specific value of prestrain is not mentioned. Then, plasma treatment and self-assembled monolayer, poly-L-lysine (PLL) treatment are utilized to enhance the wetting property. All the active layers are deposited by solution processes (inkjet-printing, spin-coating), except the thermally evaporated Al cathode. Finally, after releasing the prestrain, the microwrinkled PLEDs are obtained.

Electrical characteristics of microwrinkled PLEDs are measured only in a wrinkled state after releasing the prestrain. In **Figure 2**a,b, the microwrinkled PLEDs are prepared by fabricating on a biaxially 20% prestretched PDMS and releasing the prestrain. For comparison, a reference device, which is fabricated on flat PDMS spin-coated at 4000 rpm on glass by the same process conditions, is prepared. The wrinkled PLEDs show higher leakage current at off-state, but does not affect
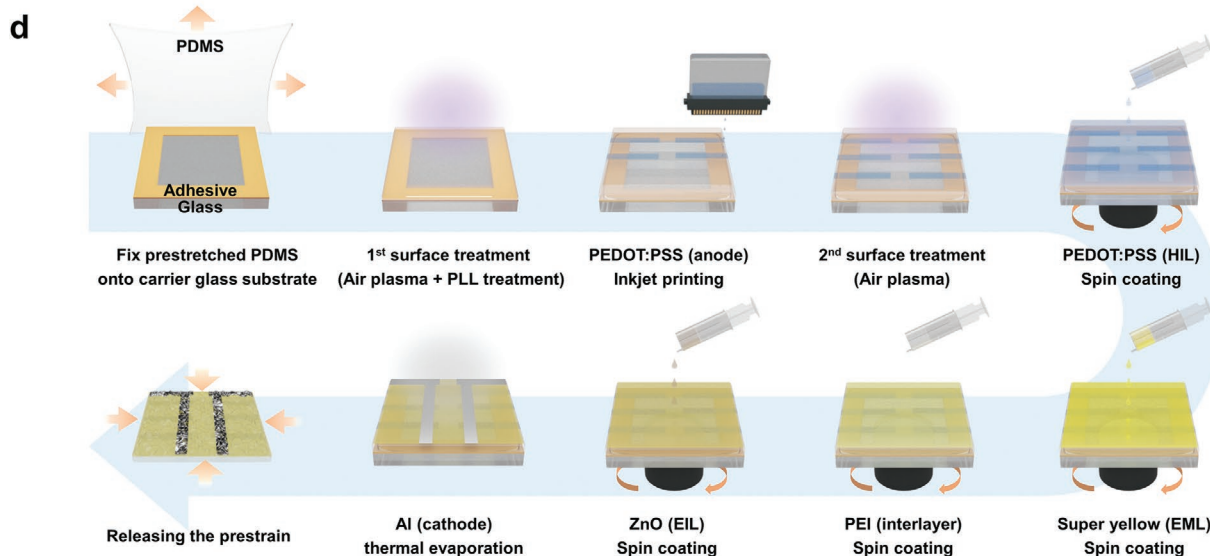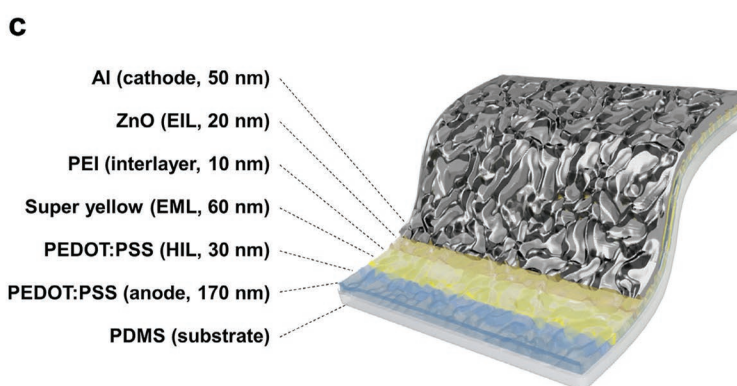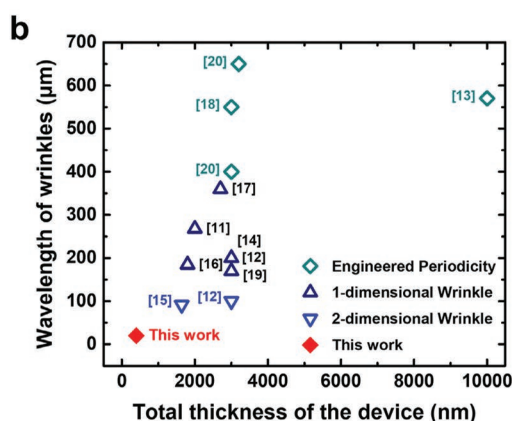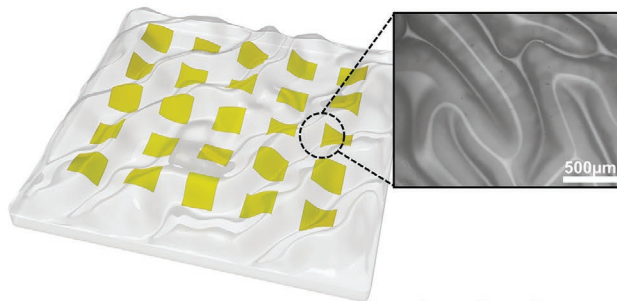
Figure 1. Stretchable OLEDs with imperceptibly microwrinkled structure. a) Schematic illustration of the concept for the formation of imperceptible/macroscopic wrinkles in stretchable OLEDs. b) Comparison with previous research reporting geometrically wrinkled stretchable TFLEDs (total thickness of the device vs wavelength of wrinkles). c) Device structure for the microwrinkled PLEDs. d) Fabrication process of microwrinkled PLEDs.

on device failure showing similar device characteristics compared to the reference device. The wrinkled PLEDs show turn-on voltage of 2.4 V, maximum luminance over 8000 cd m^{-2} at 10 V, the maximum current efficiency of 7.00 cd A^{-1}, and maximum power efficiency of 5.09 lm W^{-1}, versus 2.5 V, over 13 000 cd m^{-2}, 7.71 cd A^{-1}, and 5.24 lm W^{-1} in the reference

**ADVANCED
SCIENCE NEWS**
www.advancedsciencenews.com

**ADVANCED
MATERIALS
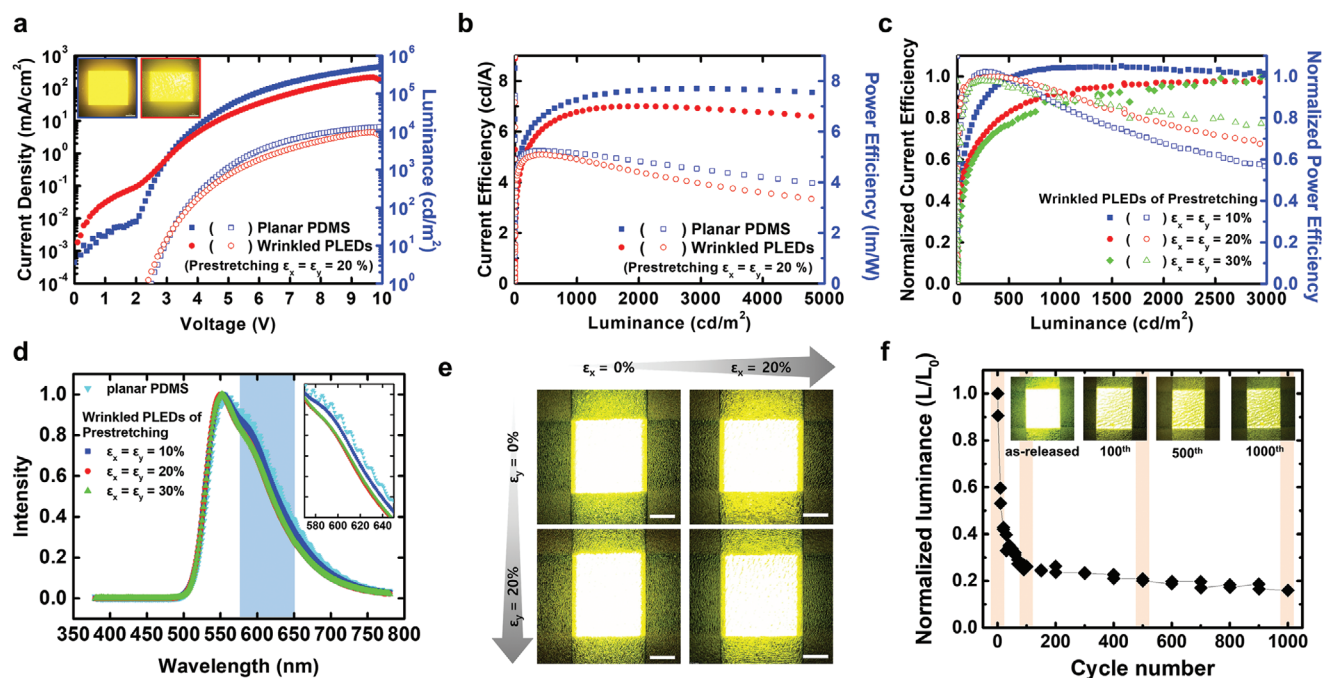TECHNOLOGIES**
www.advmattechnol.de

Figure 2. Electromechanical properties of microwrinkled PLEDs. a) *J–V–L* characteristics and b) efficiency curve of PLEDs on a planar PDMS (reference) and wrinkled PLEDs. c) Efficiency depending on the prestretching ratios normalized by the wrinkled PLEDs fabricated on biaxially 20% prestrained PDMS. d) Electroluminescence spectrum depending on the prestretching ratios. e) Biaxial stretching image of microwrinkled PLEDs (Scale bar: 0.5 mm). f) Biaxial 10% stretching cycle test of 1000 cycles. The insets are light-emitting images at cycle number of 0, 100, 500, and 1000 in the order from the left.

device, respectively. In Figure 2c, electrical characteristics depending on the prestretching ratio were confirmed. The wrinkle topography is affected by the prestretching ratio, as will be described next. The samples with biaxial prestretching of 10%, 20%, and 30% were prepared, and the data are normalized to the biaxially 20% prestretched sample. Although the wrinkled topography is formed differently, the current efficiency exhibits a similar trend. However, spectrum data show that the peak becomes narrower when the wrinkle is formed, especially as the prestretching ratio is increased (Figure 2d). This spectral change is attributed to the microcavity effect.[15,29,30] The wrinkled structure changes the traveling path of the light to be lengthened depending on the slope of the wrinkle, resulting in the resonance peak to be little blueshifted.

To evaluate the mechanical characteristics, stretching test is carried out in a glove box. The pixel of the wrinkled PLEDs shows normal light emission under stretching at 20% in *x*-axis, 20% in *y*-axis, and 20% both in *x*- and *y*-axis (Figure 2e). And stretching cycle test is conducted by stretching 10% both in *x*- and *y*-axis, while a bias condition is fixed to 0.5 mA current-driving mode. In Figure 2f, the normalized luminance dramatically decreases in the first 100 times, but the pixel maintains its emissive property even after 1000 times of cycles at the defined pixel areas. In the emission image, it is observed that the nonemissive black lines and spots appear to gradually expand as the cycle test proceeds. One of the plausible causes seems to be the delamination at the metal/polymer interface due to the weak interfacial adhesion.[31–33] The nonemissive areas appear at the initial stage of as-released wrinkled PLEDs which can be observed in highly magnified optical images (Figure S1 in

the Supporting Information), propagating spatially as the cyclic stress is accumulated. So, altering the cathode to more flexible materials such as organic-based materials would improve the mechanical properties.[34]

Morphology of wrinkled structure depending on the prestretching percentage is as follows in **Figure 3**a. Randomly oriented wrinkles are formed at the entire surfaces, and among them, herringbone-patterned wrinkle is plotted as a representative image for ease of distinguishing the differences. Distribution of wavelength between the wrinkles is analyzed by image processing through a custom-made code written in Matlab (Figure S2 in the Supporting Information), and the results are illustrated by histograms in Figure 3b. The histogram shows that the wavelength of wrinkles is all less than 25 μm at different prestretching ratios. The human eye is known to have an angular resolution of about 1/60° under normal lighting conditions.[35,36] The distance resolution is calculated by the following Equation (2)

$$s = 2 \cdot d \cdot \tan(\theta/2) \qquad (2)$$

where *s* is the distance resolution, *d* is the viewing distance between observer and object, and *θ* is the angular resolution in radians. The viewing distance for resolving the spacing of 25 μm is calculated as 8.59 cm, which is much shorter than the general viewing distance for display applications.[36] When considering that the most dominant peak in the distribution of wrinkles is much smaller, its viewing distance for resolving the wrinkles should become much shorter. Therefore, the wrinkles cannot be perceived by naked human eyes by its resolving limit in a psychophysical manner.
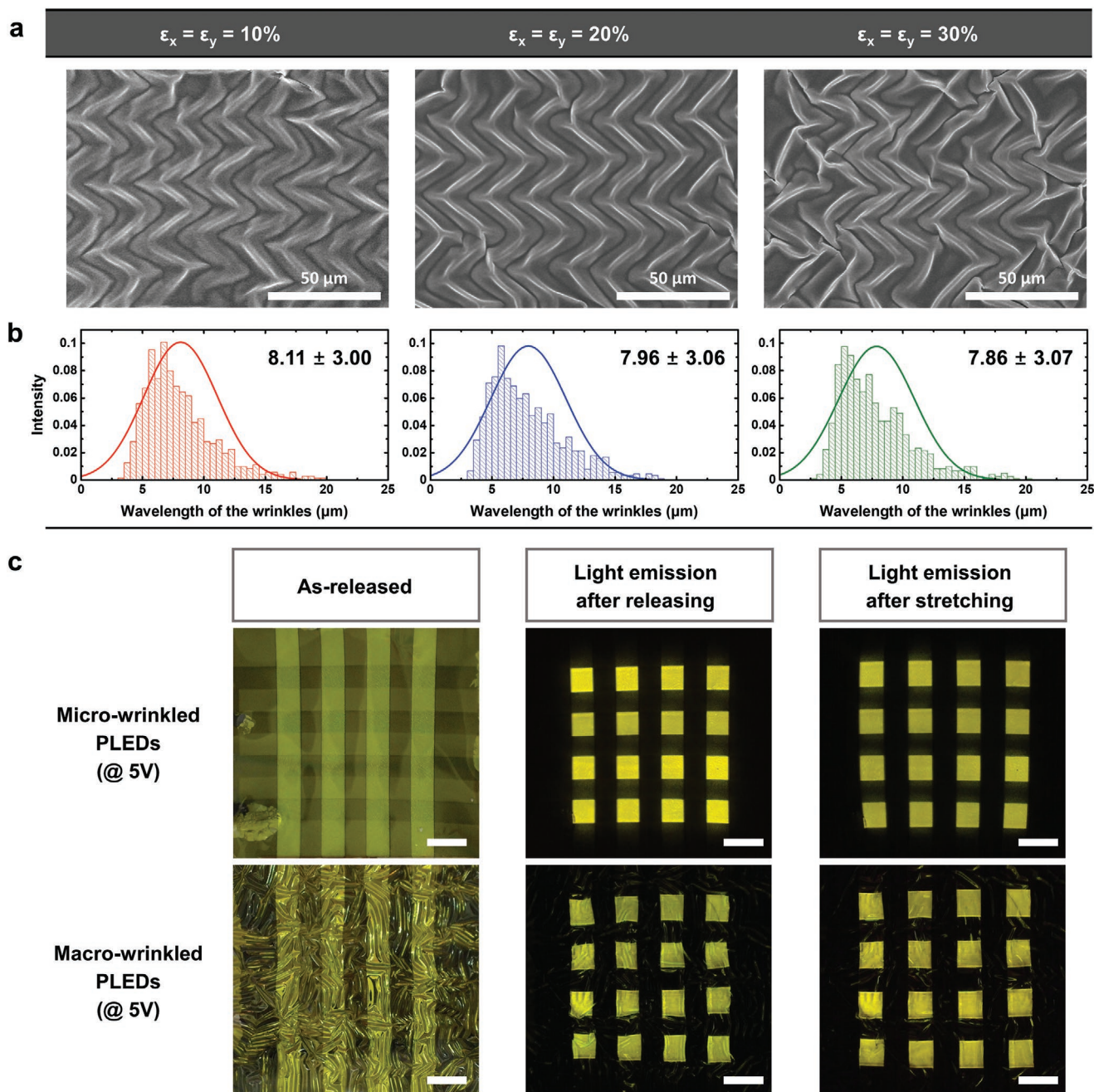
Figure 3. Topography of microwrinkled structure and demonstration for distortion-free pixel arrays. a) FESEM image of microwrinkled topography depending on the prestretching ratio. b) Histogram for the distribution of the wavelength of the wrinkles depending on the prestretching ratio. c) Demonstration of distortion-free pixel arrays. Microwrinkled PLEDs (up) and macrowrinkled PLEDs (down) are plotted together (Scale bar: 2 mm).

In Figure 3b, a histogram fitted with Gaussian distribution shows mean values of 8.11, 7.96, and 7.86 µm, respectively, which has almost no differences. When assuming that the overall shape of the wrinkles follows a 1D sinusoidal wave having the wavelength of the above mean value and can be stretched only in a single axis up to 10%, 20%, and 30%, each, the amplitudes can be calculated as 0.84, 1.21, and 1.51 µm, respectively.[16] Therefore, as the prestretching ratio increases, the aspect ratio of the wrinkle also increases, causing higher bending stress to the film (Figure S3 in the Supporting Information). It is

generally known that the stretchability increases proportionally to the prestretching ratio. However, the above data show that the film would experience more stress as the prestretching ratio increases. Consequently, there may be partial points where the stress is concentrated to relieve this stress, which can lead to delamination or crack, which will adversely affect the overall mechanical stability. Therefore, it is necessary to understand the trade-off relationship and optimize the fabrication conditions considering the material properties and the thickness of the film for the target stretchability.

Finally, distortion-free pixel arrays are demonstrated based on the microwrinkled PLEDs. For direct comparison with the conventional method, large-scale wrinkled PLEDs with an ultrathin plastic film are also fabricated by utilizing spin-coated PI varnish having a thickness of 5 μm (Figure S4 in the Supporting Information). On the ultrathin PI film, PLEDs are deposited using the same fabrication process, transferred to prestretched elastomeric substrate of 3M VHB 4905 tape, and released to form wrinkled structure, which is denoted as macrowrinkled PLEDs from below. Prestretching ratio is set to be biaxial 20% in both devices. Here, when a thickness of the prestretched elastomeric substrate is not thick enough, a global buckling appears to prevent the formation of wrinkles that endow the stretchability of the system.[37] Especially in macrowrinkled PLEDs, increase of substrate thickness is necessary to shift the wrinkle formation state from the global buckling to local buckling, which can result in limit in designing the overall thickness of devices in stretchable applications.

The optical image is pictured inside the glove box using a microscope of 20× magnification (Figure 3c). The macrowrinkled PLEDs show the wavelength of wrinkles to be 200 μm, where the surface topography can be observed along the curvature of the wrinkled structure when it is under low bias conditions. Moreover, randomly generated bidirectional wrinkles distort the shape of the pixels and do not maintain the initial square patterns. In microwrinkled PLEDs, a 4 × 4 pixel array shows a clear square pattern even after releasing the prestrain, and an invisible microwrinkle enables to define distortion-free pixel before and after stretching. Microwrinkled PLEDs seem intrinsically stretchable by invisible wrinkled structure, opening the possibility of high-resolution display applications without areal loss caused by interconnects, achieving its high device performance based on the conventional device structure with high efficiency and low operation voltage.

In this work, imperceptibly microwrinkled PLEDs for stretchable applications are suggested as a breakthrough in the conventionally established material-, structural-based studies by a simple optical trick of introducing the microwrinkles. Formation of macroscopic wrinkles has been discussed as a drawback in wrinkled stretchable devices so far, but the formation of fine wrinkles has not been mentioned as a controllable variable due to the limitations in the fabrication process. In that the scale of wrinkle structure has evolved into a controllable factor, this paper opened a new chapter in stretchable LED technologies. In this paper, what advantages can be obtained by the formation of microwrinkled PLEDs are discussed and direct deposition method of PLEDs on PDMS has been suggested, improving the yield issues related to the complex transfer process and defining distortion-free light-emitting pixels by the formation of microwrinkled structure without the aid of plastic films. This approach that is advantageous in terms of high device performance and visual aspects, is expected to enable the realization of stretchable display with high-resolution and high definition properties. Though we simply deposited PLEDs on biaxially prestretched substrate, there is much room for improvements in electromechanical characteristics when materials and structural design are complemented. Further investigation about not only various candidates for highly flexible or transparent electrodes (silver nanowires, graphene, etc.) and

active layers, but also the mechanical analysis or optimization of microwrinkled structure need to be followed as future work. Meanwhile, encapsulation is essential for practical application of OLEDs and the thickness of encapsulation layer should be considered as well in the formation of microwrinkles. However, the formation of microwrinkles in the encapsulation layer is a problem directly related to stretchable encapsulation and research on stretchable encapsulation has not yet been reported due to technical issues. Although it is difficult to further discuss the feasibility at this stage, an appropriate stretchable encapsulation technology has to be selected for microwrinkle formation. Nevertheless, the development of encapsulation method would advance the commercialization of a stretchable display making a synergetic effect with the suggested approach. Our in situ fabrication method for the microwrinkled PLEDs can become a new framework for stretchable LEDs in terms of simple fabrication process, high device performance, and improved visibility and stretchable displays having highly defined resolution in free-form display and wearable device application can be realized in the future.

Experimental Section

Substrate Preparation: A PDMS mixture (Sylgard 184, Dow Corning Corp.) was prepared by mixing the base and the curing agent in a weight ratio of 10:1. The PDMS mixture was spin-coated on a soda-lime glass with spin speed of 300 rpm for 1 min, and thermally cured at 100 °C for 90 min. Fully cured PDMS was peeled off from the glass and fixed on the biaxially stretchable jig to prestretch the PDMS up to a fixed percentage and the prestretched PDMS was transferred to a flat carrier glass having adhesives at all corners, so that the PLEDs can be fabricated not in a floating state.

Solution Process-Based PLEDs Fabrication: To overcome the hydrophobic property of PDMS, a self-assembled monolayer of PLL was drop-casted on PDMS after air plasma treatment (CUTE-1MP, Femto Science) and rinsed to remove the residues. Highly conductive PEDOT:PSS (IJ-1005, Orgacon) was inkjet-printed on PLL-treated PDMS as anode using a piezoelectric inkjet printing system (DMP-2831, Fujifilm Dimatix Corp.). The patterned PEDOT:PSS film was dried at 100 °C for 1 h. Afterward, a surface modification using air plasma was treated again to enhance the wetting property and the samples were moved to an Ar-filled glove box to proceed the deposition of other active layers. The hole injection layer of PEDOT:PSS (AI4083, Heraeus) was spin-coated at 2000 rpm for 60 s and dried at 100 °C for 30 min. The emission layer of super yellow (0.6 wt% in toluene, PDY-132, Merck) was spin-coated at 2000 rpm for 60 s and dried at 90 °C for 1 h. The PEI (0.1 wt% in IPA, Sigma-Aldrich) was spin-coated at 5000 rpm for 50 s and dried at 100 °C for 10 min. For the electron injection layer, ZnO nanoparticles (10:1 diluted in volume in butanol, N-13, Avantama) were spin-coated at 4000 rpm for 30 s and dried at 120 °C for 10 min. A thin metal mask patterned perpendicularly to the inkjet-printed PEDOT:PSS anode was aligned to the samples, and the samples were moved into the vacuum chamber. When the vacuum state became high enough, aluminum (Al) cathode was thermally evaporated with a thickness of 50 nm. Finally, by cutting along the edge of the adhesive, the prestretched sample shrinks to its original length, forming microwrinkles on the whole surfaces.

Encapsulation: To protect the PLEDs from the ambient conditions during the electrical characterization, the wrinkled PLEDs were aligned to the inkjet-printed silver (JET-004T, Kunshan Hisense Electronic Corp.) contact pad and the encapsulation glass was covered to isolate the wrinkled PLEDs from the outside. The encapsulation glass was firmly adhered by using a UV-curable epoxy (XNR5570, Nagase ChemteX Corp.).

Measurement: The thickness of the PLEDs was characterized using an atomic force microscope (AFM, XE-100, Parks' System Corp.) by measuring the step between the layers. Electrooptical properties were

measured by a spectrometer (CS-1000A, Konica Minolta) by calibrating the data by the pixel size, and a digital multimeter (Keithley 2000, Keithley) and a source-measurement unit (Keithley 237, Keithley) by sweeping the voltage with an interval of 0.1 V, respectively. It is noted that J–V–L and efficiency characteristics were measured for the microwrinkled PLEDs in the released state. Stretching cycle test was carried out inside the glove box and the luminance was measured by a spectrometer (CS-200, Konica Minolta) at a fixed position outside the glove box. The optical images of light emission were obtained with a digital microscope (DSX510, Olympus Corp.) and handheld digital microscope (AM4515T, AnMo Electronics Corp.). Surface topography of the microwrinkled PLEDs was pictured by a field emission scanning electron microscope (FESEM, S-4800, Hitachi).

Supporting Information

Supporting Information is available from the Wiley Online Library or from the author.

Conflict of Interest

The authors declare no conflict of interest.

[1] J.-H. Hong, J. M. Shin, G. M. Kim, H. Joo, G. S. Park, I. B. Hwang, M. W. Kim, W. S. Park, H. Y. Chu, S. Kim, *J. Soc. Inf. Disp.* **2017**, *25*, 194.

[2] S. Kim, J. M. Shin, J.-H. Hong, G. S. Park, H. Joo, J. H. Park, G. Lee, J. Yoon, H. Shin, S.-C. Jo, C. Lee, J. Kwag, *SID Symp. Dig. Tech. Pap.* **2019**, *50*, 1194.

[3] S. Kwon, Y. H. Hwang, M. Nam, H. Chae, H. S. Lee, Y. Jeon, S. Lee, C. Y. Kim, S. Choi, E. G. Jeong, K. C. Choi, *Adv. Mater.* **2020**, *32*, 1903488.

[4] J. Park, D. B. Ahn, J. Kim, E. Cha, B.-S. Bae, S.-Y. Lee, J.-U. Park, *Sci. Adv.* **2019**, *5*, eaay0764.

[5] J. Liang, L. Li, X. Niu, Z. Yu, Q. Pei, *Nat. Photonics* **2013**, *7*, 817.

[6] Z. Zhang, K. Guo, Y. Li, X. Li, G. Guan, H. Li, Y. Luo, F. Zhao, Q. Zhang, B. Wei, Q. Pei, H. Peng, *Nat. Photonics* **2015**, *9*, 233.

[7] J. Wang, C. Yan, K. J. Chee, P. S. Lee, *Adv. Mater.* **2015**, *27*, 2876.

[8] R.-H. Kim, D.-H. Kim, J. Xiao, B. H. Kim, S.-I. Park, B. Panilaitis, R. Ghaffari, J. Yao, M. Li, Z. Liu, V. Malyarchuk, D. G. Kim, A.-P. Le, R. G. Nuzzo, D. L. Kaplan, F. G. Omenetto, Y. Huang, Z. Kang, J. A. Rogers, *Nat. Mater.* **2010**, *9*, 929.

[9] T. Sekitani, H. Nakajima, H. Maeda, T. Fukushima, T. Aida, K. Hata, T. Someya, *Nat. Mater.* **2009**, *8*, 494.

[10] J. Byun, E. Oh, B. Lee, S. Kim, S. Lee, Y. Hong, *Adv. Funct. Mater.* **2017**, *27*, 1701912.

[11] M. S. White, M. Kaltenbrunner, E. D. Głowacki, K. Gutnichenko, G. Kettlgruber, I. Graz, S. Aazou, C. Ulbricht, D. A. Egbe, M. C. Miron, Z. Major, M. C. Scharber, T. Sekitani, T. Someya, S. Bauer, N. S. Sariciftci, *Nat. Photonics* **2013**, *7*, 811.

[12] D. Yin, J. Feng, N.-R. Jiang, R. Ma, Y.-F. Liu, H.-B. Sun, *ACS Appl. Mater. Interfaces* **2016**, *8*, 31166.

[13] D. Yin, J. Feng, R. Ma, Y.-F. Liu, Y.-L. Zhang, X.-L. Zhang, Y.-G. Bi, Q.-D. Chen, H.-B. Sun, *Nat. Commun.* **2016**, *7*, 11573.

[14] T. Yokota, P. Zalar, M. Kaltenbrunner, H. Jinno, N. Matsuhisa, H. Kitanosako, Y. Tachibana, W. Yukita, M. Koizumi, T. Someya, *Sci. Adv.* **2016**, *2*, e1501856.

[15] H. Hafeez, Z. Zou, D. H. Kim, J. Y. Shin, M. Song, C.-S. Kim, W. J. Choi, J. Song, J. Xiao, S. Y. Ryu, *Org. Electron.* **2017**, *48*, 314.

[16] T.-H. Kim, C.-S. Lee, S. Kim, J. Hur, S. Lee, K. W. Shin, Y.-Z. Yoon, M. K. Choi, J. Yang, D.-H. Kim, T. Hyeon, S. Park, S. Hwang, *ACS Nano* **2017**, *11*, 5992.

[17] M. K. Choi, J. Yang, D. C. Kim, Z. Dai, J. Kim, H. Seung, V. S. Kale, S. J. Sung, C. R. Park, N. Lu, T. Hyeon, D.-H. Kim, *Adv. Mater.* **2018**, *30*, 1703279.

[18] D. Yin, N.-R. Jiang, Y.-F. Liu, X.-L. Zhang, A.-W. Li, J. Feng, H.-B. Sun, *Light: Sci. Appl.* **2018**, *7*, 35.

[19] Y. F. Li, S. Y. Chou, P. Huang, C. Xiao, X. Liu, Y. Xie, F. Zhao, Y. Huang, J. Feng, H. Zhong, H.-B. Sun, Q. Pei, *Adv. Mater.* **2019**, *31*, 1807516.

[20] D. Yin, N.-R. Jiang, Z.-Y. Chen, Y.-F. Liu, Y.-G. Bi, X.-L. Zhang, J. Feng, H.-B. Sun, *Adv. Opt. Mater.* **2020**, *8*, 1901525.

[21] D. Jiin, S. An, H. Kim, Y. Kim, H. Koo, T. Kim, Y. Kim, H. Min, S. Kim, *SID Symp. Dig. Tech. Pap.* **2011**, *42*, 492.

[22] Z. Y. Huang, W. Hong, Z. Suo, *J. Mech. Phys. Solids* **2005**, *53*, 2101.

[23] Y. Wang, Z. Li, J. Xiao, *J. Electron. Packag.* **2016**, *138*, 020801.

[24] J. Song, H. Jiang, W. M. Choi, D. Y. Khang, Y. Huang, J. A. Rogers, *J. Appl. Phys.* **2008**, *103*, 014303.

[25] J. Lee, S. Chung, H. Song, S. Kim, Y. Hong, *J. Phys. D: Appl. Phys.* **2013**, *46*, 105305.

[26] N. Bowden, S. Brittain, A. G. Evans, J. W. Hutchinson, G. M. Whitesides, *Nature* **1998**, *393*, 146.

[27] T. Q. Trung, C. Kim, H.-B. Lee, S. M. Cho, N.-E. Lee, *Adv. Mater. Technol.* **2020**, *5*, 1900995.

[28] J. Zhou, A. V. Ellis, N. H. Voelcker, *Electrophoresis* **2010**, *31*, 2.

[29] B.-W. Lee, Y.-G. Ju, *Opt. Quantum Electron.* **2009**, *41*, 627.

[30] J. Moon, E. Kim, S. K. Park, K. Lee, J.-W. Shin, D.-H. Cho, J. Lee, C. W. Joo, N. S. Cho, J.-H. Han, B.-G. Yu, S. Yoo, J.-I. Lee, *Org. Electron.* **2015**, *26*, 273.

[31] A. J. Nolte, J. Y. Chung, C. S. Davis, C. M. Stafford, *Soft Matter* **2017**, *13*, 7930.

[32] Y. Liu, X. Wang, Y. Xu, Z. Xue, Y. Zhang, X. Ning, X. Cheng, Y. Xue, D. Lu, Q. Zhang, F. Zhang, J. Liu, X. Guo, K.-C. Hwang, Y. Huang, J. A. Rogers, Y. Zhang, *Proc. Natl. Acad. Sci. USA* **2019**, *116*, 15368.

[33] J. Hora, C. Hall, D. Evans, E. Charrault, *Adv. Eng. Mater.* **2018**, *20*, 1700868.

[34] J. Park, H. Yoon, G. Kim, B. Lee, S. Lee, S. Jeong, T. Kim, J. Seo, S. Chung, Y. Hong, *Adv. Funct. Mater.* **2019**, *29*, 1902412.

[35] M. E. Becker, *SID Symp. Dig. Tech. Pap.* **2017**, *48*, 915.

[36] S. Lee, S. Lee, H. Yoon, C.-K. Lee, C. Yoo, J. Park, J. Byun, G. Kim, B. Lee, B. Lee, Y. Hong, *Opt. Express* **2018**, *26*, 824.

[37] S. Wang, J. Song, D.-H. Kim, Y. Huang, J. A. Rogers, *Appl. Phys. Lett.* **2008**, *93*, 023126.